Automated operational forecasting of monsoon low pressure systems

D.L. Suhas[1] , S. Vishnu[2,3] , Salil Goyal[4] , Sahadat Sarkar[5] , Parthasarathi Mukhopadhyay[5] , Paul A. Ullrich[6,7] , William R. Boos[1,8*]

[1] *Department of Earth and Planetary Science, University of California, Berkeley, USA*

[2] *Direction de la Climatologie et des Services Climatiques, Météo-France, Toulouse, France*

[3] *Institute de Recherche pour le Développement (IRD), Nouméa, Nouvelle-Calédonie*

[4] *Department of Mathematics, University of California, Berkeley, USA*

[5] *Indian Institute of Tropical Meteorology, Ministry of Earth Sciences, Pune, India*

[6] *Department of Land, Air and Water Resources, University of California, Davis, USA*

[7] *Computational Research Division, Lawrence Berkeley National Laboratory, Berkeley, USA*

[8] *Climate and Ecosystem Sciences Division, Lawrence Berkeley National Laboratory, Berkeley, USA*

[*] *Corresponding author*: William R. Boos, william.boos@berkeley.edu

ABSTRACT: Monsoon low pressure systems (LPS) are the dominant rain-bearing weather system of the densely populated South Asian region, often producing extreme precipitation and hydrological disasters. Despite the importance of these storms, no operational system has automatically identified and tracked LPS in real time in numerical weather prediction model output. Here, we describe a new system, developed by an international partnership, that uses tailored algorithms to identify South Asian LPS in short-term forecasts from the U.S. Global Forecast System (GFS-US) and the variant of the GFS model used operationally by the Indian Institute of Tropical Meteorology (IITM). We also assess the historical performance of the control runs of these models in forecasting monsoon LPS across South Asia, and compare this with the performance of the Integrated Forecasting System of the European Centre for Medium-Range Weather Forecasts (ECMWF). One to two days before observed LPS genesis, the models have a 35-60% probability of detecting the storm, with a 35-55% false alarm ratio. For lead times up to five days, all of these models forecast LPS positions with a mean bias much smaller than typical storm outer radii. The mean model forecast predicts the storm precipitation maximum within 40% of the observed value. The GFS-US model performed more poorly than the ECMWF model in forecasts of several metrics, but its skill improved over the last 15 years to eliminate this gap. Overall, this operational system provides skillful forecasts of LPS intensities and rain rates, yielding useful information for forecasters and disaster managers in South Asia.

SIGNIFICANCE STATEMENT: The South Asian region often experiences intense rainfall and disasters produced by cyclonic vortices known as monsoon low pressure systems (LPS). In this work, we introduce the first automated operational system that uses numerical weather prediction model output with a tracking algorithm optimized for monsoon LPS to forecast the behavior of these storms. This system provides skillful forecasts of LPS positions, intensities, and rain rates, offering valuable information for forecasters and disaster managers in South Asia.

Along the banks of the Mandakini river in the western Garhwal Himalayas lies Kedarnath, a small town in the North Indian state of Uttarakhand. Summer marks its peak tourist season, drawing many pilgrims after the winter closure. On the evening of June 16, 2013, rain began pouring down on Kedarnath, triggering flash floods and causing widespread devastation (Dobhal et al. 2013). Over three days, Uttarakhand received more than 500 mm of rain (Houze et al. 2017), resulting in over 6000 deaths and affecting half a million people (Guha-Sapir et al. 2015; Sati and Gahalaut 2013). Shortly after its occurrence, this disaster was called India's worst natural calamity since the 2004 Indian Ocean tsunami (Dubey et al. 2013). Yet such hydrological extremes occur every few years in South Asia (Nikumbh et al. 2020), including intense rainfall in Mumbai in 2005 (Kumar et al. 2008), the 2010 floods in Pakistan (Houze et al. 2011), the Chennai floods of 2015 (Chakraborty 2016), and the 2018 Kerala disaster (Hunt and Menon 2020). A common thread connecting this particular list of examples is the presence of a monsoon low pressure system (LPS), a synoptic-scale vortex that produces high rain rates as it propagates over densely populated parts of South Asia during the summer monsoon (Sikka 1978). In fact, more than half of South Asia's hydro-meteorological disasters are associated with these monsoon LPS (Suhas et al. 2023).

Monsoon LPS are cyclonic vortices with typical outer diameters exceeding 2000 km, forming in the strong vertical and meridional wind shear of the summer monsoon flow over both South Asia (Mooley and Shukla 1987) and Australia (Davidson and Holland 1987). In South Asia, their genesis is highly concentrated in space, with most systems forming over the northwestern Bay of Bengal and relatively few spinning up over other areas of the North Indian Ocean (Sikka 2006). After formation, LPS typically propagate westward, producing intense rainfall over continental India during the ensuing 5-10 day storm lifetime. Peak rainfall is focused southwest of the vortex center,

in the region where vortex interaction with the background vertical shear produces dynamical uplift (Rao and Rajamani 1970; Sanders 1984). Unlike canonical tropical cyclones, these vortices have a lower-tropospheric cold core, and can also transit the continental surface without appreciable loss of intensity (Sikka 1978). They are responsible for a large fraction of annual rainfall (Godbole 1977; Yoon and Chen 2005; Hurley and Boos 2015; Hunt and Fletcher 2019), and sometimes produce extreme precipitation (Ajayamohan et al. 2010; Thomas et al. 2021) and disasters (Suhas et al. 2023) over South Asia.

Accurately forecasting the location and intensity of these storms is vital for providing early disaster warnings and ensuring disaster preparedness. While tropical cyclones are routinely identified by operational, automated algorithms in forecasts made by numerical weather prediction (NWP) systems (Cangialosi 2021; Sampson and Schrader 2000; Yu et al. 2013), no analogous effort has been made for monsoon LPS, despite the great size of the human population affected by these storms. Recent research has confirmed the potential utility of short-term LPS track and precipitation forecasts for providing early warning of hydrological disasters in South Asia (Suhas et al. 2023). Thus, there is a compelling need to establish an operational real-time forecasting system for monsoon LPS. Here we describe such a system, developed through an international partnership, that utilizes short-term forecasts from numerical weather prediction models run operationally in India and the U.S.

For operational forecasts of monsoon LPS to be of practical use, it is crucial to examine the skill of those forecasts. We are aware of only two studies that have analysed the skill of operational NWP models in forecasting monsoon LPS. Sarkar et al. (2021) found that the Global Forecast System (GFS) model used operationally by the India Meteorological Department performed well in simulating the dynamics involved in the transition of weaker LPS (called monsoon lows) to stronger vortices (called monsoon depressions), but performed more poorly in forecasting the dynamics of monsoon lows that did not intensify to depression strength. They did not assess the model's skill in predicting LPS position, intensity, or rain rate. Deoras et al. (2021) assessed South Asian monsoon LPS forecasts in the Subseasonal-to-Seasonal (S2S) prediction project, using reforecasts from 11 models for lead times up to 15 days. When compared to ERA-Interim and MERRA-2, they found that S2S models underestimated the frequency of LPS and were underdispersive in their forecasts of LPS position and intensity. However, Deoras et al. (2021) did not assess the genesis skill of the

NWP models or analyze storm-centered rain rates, and also did not examine the skill of the NWP models used operationally by Indian institutions.

The automated, real-time, operational system introduced here identifies monsoon LPS in short-term forecasts from the Global Forecast System (GFS), developed by the National Centers for Environmental Prediction (NCEP), and from a variant of the Global Forecast System run by the Indian Institute of Tropical Meteorology (GFS-IITM). To clearly distinguish the two models, we henceforth refer to the version of the GFS model run in the U.S. as the GFS-US model. We evaluate the historical performance of these models by comparing with LPS tracks from an atmospheric reanalysis; this reanalysis was previously shown to compare well with hand-analyzed track datasets of monsoon LPS (Vishnu et al. 2020). In addition to these two NWP models, we also assess the skill of the Integrated Forecasting System (IFS) of the European center for Medium-Range Weather Forecasts (ECMWF). Our assessment focuses on the models' capabilities in predicting the genesis, track location, intensity, and precipitation rates of South Asian LPS. The results presented here build on previous work by some of the authors, including optimization and validation of the LPS tracking algorithm (Vishnu et al. 2020) and assessment of the skill of an NWP ensemble in forecasting LPS genesis (Suhas and Boos 2024). The data sources and methodology that we use are described in the next section. We then discuss example forecasts from the operational system for a representative LPS, and assess the historical forecast skill of the NWP models. The paper concludes by summarizing and discussing implications of the findings.

Data and methods

Data sources

We implemented our automated tracking system for monsoon LPS for short-term forecasts from both the GFS-US and GFS-IITM models. The system also uses ensemble forecasts from the Global Ensemble Forecast System developed by NCEP, with its latest version (GEFS v12) providing 30 perturbed forecasts (Zhou et al. 2022). The GFS-US model is initialized four times a day and uses a cubed-sphere grid with a horizontal resolution of about 25 km, with 64 vertical levels on sigma-pressure hybrid layers. It employs the GFDL microphysics parameterization and the Simplified Arakawa–Schubert shallow and deep convection schemes (Zhou et al. 2022). To avoid confusion,

we refer to both the control and ensemble configurations of the Global Forecast System run in the U.S. as the GFS-US model, explicitly referencing ensemble forecasts where relevant.

The GFS-IITM model is a variant of NCEP's GFS model, which has been operational at the Indian Institute of Tropical Meteorology (IITM) since June 2016. It employs a spectral resolution of T1534 (nominally 12.5 km) with 64 hybrid vertical levels, and is initialized twice a day at 00 and 12 hours UTC to produce deterministic forecasts over India. Details on this model are provided by Mukhopadhyay et al. (2019), but we note that to represent moist convection the model uses a Revised Simplified Arakawa–Schubert (Han and Pan 2011; Ganai et al. 2016) scheme and a mass flux-based Simplified Arakawa–Schubert shallow convection scheme. India's National center for Medium Range Weather Forecasting (NCMRWF) generates initial conditions using the Global Data Assimilation System (GDAS) cycle, incorporating denser observations in the Indian region; for details, see Prasad et al. (2016).

We compare forecasts from the above two models with those from the ECMWF NWP model. However, we have not implemented operational identification and tracking of monsoon LPS in ECMWF forecasts because those forecasts are not available to the general public in real time. The ECMWF model is also spectral in nature, and its latest version has a horizontal resolution of O1280 (an octahedral grid, nominally 9 km in the horizontal) with 137 vertical levels. We obtained the ECMWF forecasts at a horizontal resolution of $0.5^\circ \times 0.5^\circ$ from the archive of The International Grand Global Ensemble (TIGGE; Bougeault et al. 2010; Swinbank et al. 2016). Further details on the ECMWF model and the TIGGE archive can be found in Park et al. (2008), but we note that it uses convection schemes by Tiedtke (1989) and Bechtold et al. (2004). It is initialized twice daily at 00 and 12 hours UTC using ECMWF 4D-Var data assimilation, employing a higher-resolution model to generate the control analysis.

To maintain consistency despite variations in spatial resolution and forecast initialization times across models, our skill analyses use the model outputs at a horizontal resolution of 0.5° and focus solely on the forecasts initiated at 00 hours UTC. We assess model skill analysis for both the GFS-US and ECMWF models over a 15-year period, from 2008 to 2022, for the monsoon season of June–September. While we would have liked to analyze performance of the GFS-IITM model over the same period, transferring the substantial volumes of data (approximately 10 GB for each model forecast time) from India to the site of the analysis in the U.S. was a major challenge. As

a result, we limited our examination of GFS-IITM forecasts to those initiated between 120 and 0 hours prior to the observed genesis time of each observed LPS in the years 2016–2022. The year 2016 marks the commencement of the GFS-IITM model's operational deployment, so this choice means that we assessed the performance of that model in forecasting every LPS observed during its first 7 years of operation.

We evaluate the performance of the NWP forecasts using LPS tracks from the ECMWF fifth-generation reanalysis (ERA5) as the reference. We also re-evaluated model performance using the Modern-Era Retrospective Analysis for Research and Applications, version 2 (MERRA-2) as the reference, since using ERA5 might confer an advantage to the ECMWF model given possible commonalities in analysis schemes and input data. However, our conclusions were relatively insensitive to this choice of reference dataset, so we only show results using ERA5 in the main text, and present a few comparisons with MERRA-2 in the online supplementary materials. To assess the skill of NWP models in forecasting LPS precipitation, we compare their precipitation forecasts with high-resolution ($0.1^\circ \times 0.1^\circ$), half-hourly precipitation estimates from the Integrated Multi-satellitE Retrievals for GPM (IMERG; Huffman et al. 2015).

Algorithms for identifying and comparing LPS tracks

The tracks of monsoon LPS in the NWP forecasts are identified using the methodology developed by Vishnu et al. (2020). They used an objective algorithm based on the TempestExtremes software (Ullrich et al. 2021) to identify LPS tracks in five reanalyses, creating the ERA5 and MERRA-2 track datasets used in this study as reference datasets. This algorithm tracks LPS using the streamfunction of the lower-tropospheric horizontal wind, a variable that is much smoother and less resolution-dependent than vorticity (which is more commonly used to track atmospheric vortices), but is not subject to assumptions of geostrophic balance like mean sea level pressure. Use of the streamfunction as the tracking variable also makes the algorithm relatively insensitive to the horizontal resolution of the input data. The identified LPS are classified by intensity as monsoon lows (weaker LPS) or monsoon depressions (a category that here includes all LPS stronger than monsoon lows); this classification is performed based on the peak surface wind speed and minimum mean sea level pressure (MSLP) anomaly achieved in a storm, following traditional criteria used by the India Meteorological Department (Vishnu et al. 2020; Ajayamohan et al. 2010). The algorithm

requires a minimum lower-tropospheric relative humidity to be achieved along the track of an LPS, to distinguish these systems from desert heat lows; as the GFS-US model systematically underestimates lower-tropospheric relative humidity over India (Mukhopadhyay et al. 2019), we used a relative humidity threshold of 80%, instead of the default 85%, to identify LPS in the GFS-US and GFS-IITM models.

The LPS tracks identified by this algorithm in 40 years of reanalysis data agree well with tracks obtained by expert hand analysis of historical MSLP maps (Vishnu et al. 2020). The algorithm also successfully identified monsoon lows and depressions in a suite of high-resolution global climate models (Vishnu et al. 2023a), even though the lows can be difficult to detect because of their weak amplitude. More details regarding this tracking algorithm and its tuning against a historical reference LPS dataset can be found in Vishnu et al. (2020).

A track in an NWP forecast is considered a match to one in the reference dataset if the spatial separation between the first four points of the NWP track that coincide in time with the reference track and the corresponding points in the reference track is less than 4° (Froude 2010; Hodges and Emerton 2015; Deoras et al. 2021). Furthermore, we require model forecast tracks to have their genesis within five days of the model initialization, thereby eliminating forecasts where genesis is predicted with a lead time of over five days. Our analyses will show that genesis-relevant metrics, such as the probability of detection and the false alarm ratio, reach values indicative of poor skill by five days of lead time. In cases where multiple tracks for a given model initialization time match the same reference track, we select the model track with genesis closest in time to that of the reference LPS genesis (Zhang et al. 2023). Additionally, if a model's LPS track matches multiple reference tracks, we choose the reference track with the minimum mean spatial separation from the model forecast.

In our analysis of model skill, we use three different time variables: forecast lead time, time prior to observed genesis, and observed time (i.e., real wall-clock time). Forecast lead time is the number of hours (or days) that have elapsed since the initialization of the forecast model, a commonly used quantity in many analyses of forecast skill, and one that we use in most of our metrics. However, when estimating the likelihood of a model forecasting the genesis of an observed LPS, we use the number of hours prior to the observed genesis time; a given time prior to observed genesis can include models with multiple forecast lead times.

Operational workflow

Our system presents operational LPS forecasts based on both the GFS-IITM and GFS-US models, with NWP model integration and subsequent processing performed in both India and the U.S. The GFS-IITM model is run operationally every day by the Indian Institute of Tropical Meteorology (IITM). Automated scripts developed at UC Berkeley were then transferred to IITM together with the tracking algorithm, where they are executed daily on an IITM high-performance computing cluster to transform pressure-level winds into the horizontal streamfunction, extract other needed variables (e.g. precipitation and surface wind speed), and identify LPS tracks. Graphics displaying the forecasts are also automatically created, then transferred to a website hosted by UC Berkeley (`http://worldmonsoons.org/LPStrackingSite/`) and also posted on the IITM short-range prediction site (`https://srf.tropmet.res.in/srf/hires_gefs/files/gfs_lps.php`).

The same workflow is performed at UC Berkeley using the control and ensemble output from the GFS-US model (run operationally at NCEP), then displayed on a separate web page (`http://worldmonsoons.org/LPStrackingSite/index_gefs.html`) on the same UC Berkeley website. The graphics on this page differ from those on the GFS-IITM page in that they incorporate track probabilities and ensemble predictions for LPS intensities and rain rates. Having access to forecasts from multiple models is usually desirable for human forecasters, which motivates our use of these parallel workflows for both the GFS-IITM and GFS-US models.

A case study of operational forecasts

We now demonstrate the functionality of our operational tracking system, and the website that displays its results, using a recent monsoon LPS that formed on 24 June 2023. According to ERA5 data, this LPS had its genesis in the northwestern Bay of Bengal at 00 UTC on June 24, as depicted by the dot at the end of the gray line in Figure 1a. Over the subsequent days, it propagated northwestward, producing extreme rainfall across central and northern India (ANI 2023; The Weather Channel 2023). The resulting floods affected over 250,000 individuals, leading to more than 200 fatalities and 600 injuries, as documented in the Emergency Events Database (EM-DAT; Guha-Sapir et al. 2015; Times 2023). The India Meteorological Department initially identified it as a weak cyclonic circulation forming over the northwestern Bay of Bengal at 0845 UTC 23 June 2023 (IMD 2023a). They issued a warning the following day at 0830 UTC 24 June 2023—eight

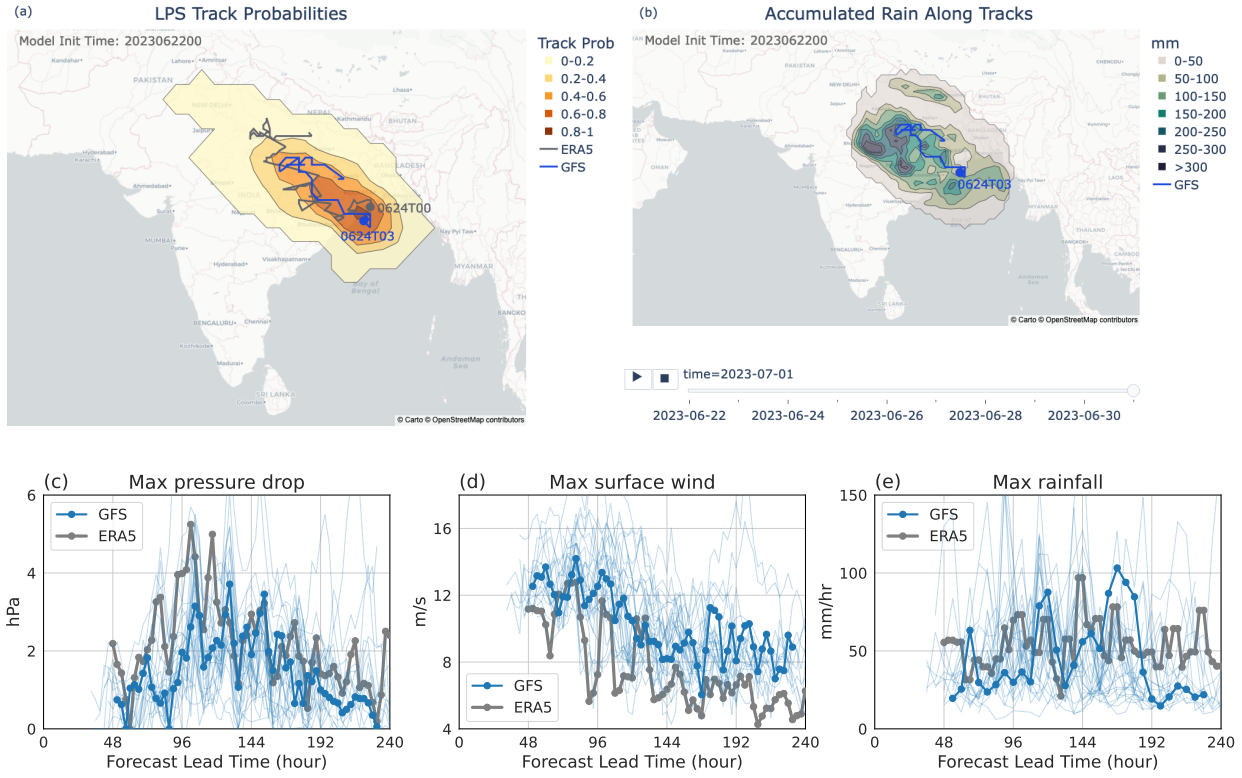

FIG. 1. Snapshot of the operational tracking website for an example LPS. Top panels show (a) track probabilities and (b) accumulated rain along the LPS tracks for ensemble GFS-US forecasts issued at 00 UTC 22 June 2023, two days prior to the observed genesis in ERA5. Track probability shows the fraction of ensemble members that pass within 1° of each point over the 10 days following model initialization. The LPS track from the GFS-US control run is shown in blue, while the corresponding ERA5 track is in gray. Genesis locations are marked by circles with corresponding genesis times. Accumulated rain is the time-integrated precipitation falling within 5° of the vortex center, from the GFS-US control run. On the website, the time-evolution in rain accumulation can be visualized using the slider below the map; here, the static map shows rain accumulated over the 10 days since forecast initialization. Bottom panels show forecasts of three intensity metrics: (c) maximum pressure drop between the vortex center and its surroundings, (d) maximum surface wind speed within 3° of the vortex center, and (e) maximum rainfall within 5° of the vortex center, all from GFS-US forecasts initialized 00 UTC of June 22, 2023. The solid blue line represents the forecast from the control run, while ensemble members are shown by thin blue lines. Vortex-centered values from observationally based datasets are shown in gray; pressure drop and wind speed are derived from ERA5, and precipitation from IMERG.

hours after its genesis in ERA5 data—suggesting a high likelihood of its intensification into an LPS (IMD 2023b).

The NWP models predicted the formation of this LPS with multiple days of additional lead time. The control run of the GFS-US model that was initialized at 00 UTC June 22, 48 hours prior to the genesis in ERA5 data, predicted genesis of this LPS on 03 UTC June 24, within about 1° of the location of observed genesis (blue line in Figure 1a). Most GFS-US ensemble members with the same initialization time also predicted this LPS genesis; the track probability, indicating the fraction of ensemble members projecting the passage of an LPS track within 1° of each point, exceeds 0.8 near the region of observed genesis. As expected, the track probability diminishes as we advance in time and move horizontally away from the genesis region, due to the spatial divergence of tracks with increased forecast lead time. The interactive map on the website displays the track probability overlaid with forecast tracks from the control run, allowing users to zoom in or out for more detailed spatial views. Hovering one's pointer over the tracks reveals the latitude, longitude, and time of the corresponding vortex center.

The NWP models also predicted that this LPS would produce heavy precipitation over central and northern India following its genesis (Figure 1b). In certain geographic areas, the forecast cumulative precipitation associated with the LPS event exceeded 300 mm.

Forecasts of the intensity of this LPS, issued two days prior to its observed genesis, were also fairly accurate. Forecasts of the maximum pressure drop of the vortex center, the maximum surface wind speed within 3° of the vortex center, and the maximum rainfall within 5° of the vortex center, all from the GFS-US model, are shown in Figures 1 c-e. Here, the maximum pressure drop measures the intensity of the MSLP minimum near the storm center; it is the magnitude of the largest closed contour of MSLP anomaly that can be drawn within a 10° radius of the vortex's minimum MSLP, with that minimum located within 3° of the vortex center (the vortex center, in turn, is the minimum of the 850 hPa streamfunction, and the MSLP anomaly is evaluated relative to this MSLP minimum). The control run is depicted by the thick blue line, while individual ensemble members are shown as thin blue lines, and these predictions are compared with ERA5 winds and MSLP, and the IMERG precipitation. While most ensemble members underestimated the pressure drop and overestimated peak surface wind speeds of the LPS, the observed value falls within the spread of the ensemble members for most forecast lead times. The GFS-US control and

ensemble even correctly projected extreme precipitation rates to exceed 50 mm hr^{-1} over central India six to eight days after model initialization (Figure 1e).

Skill of model forecasts

Having provided a case study of forecasts of a damaging monsoon LPS, we now systematically assess the numerical model skill in forecasting the behavior of monsoon LPS across South Asia. Specifically, we evaluate the skill with which the NWP models forecast the position, intensity, and rain rates of these LPS over a 15-year period spanning 2008-2022, using ERA5 tracks as a reference. As GFS-IITM has been in operational use since 2016, we evaluate its skill from that year onward. Here we focus on the skill of the control run of the GFS-US, GFS-IITM, and ECMWF models. In separate work, we assess the accuracy of forecast probabilities inferred from the GFS-US and ECMWF ensembles, and show that the control runs of those models have a higher skill in many metrics than the ensemble mean.

Spatial climatologies of LPS genesis and track densities from the GFS-US and ECMWF forecasts closely resemble those from the ERA5 reanalysis. To quantitatively compare ERA5 data with NWP forecasts initialized at multiple times, we only consider model tracks with genesis occurring within 6 to 120 hours from the time of model initialization, and then divide by the number of model initializations within this period (i.e., 5). The peak in LPS genesis occurs over the northwestern Bay of Bengal and adjacent land regions in both NWP models and in ERA5 (black contours in Figure 2). After formation, LPS typically propagate northwestward over central and western India (as indicated by the shaded track density in Figure 2). The genesis and track densities shown here also comprises of the NWP models failing to forecast some observed LPS and incorrectly forecasting others that are not observed to form (i.e., false alarms; this is examined in detail below), and the ECMWF model seems to be more cyclogenetic than observations. However, our main point here is that the NWP models overall predict roughly the correct number of LPS forming in the correct locations each summer, and subsequently propagating in the correct direction with correct termination locations.

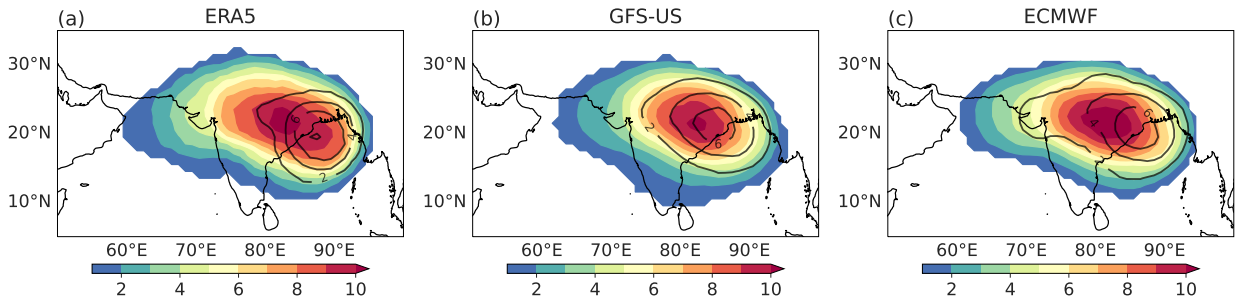

FIG. 2. The climatology of LPS genesis density (black contours) and track density (color shading) for (a) ERA5, (b) GFS-US, and (c) ECMWF models. These densities are the number of LPS genesis and track points lying within a 5° radius of each grid point during the June to September season, averaged over all years within 2008–2022. To allow comparison of ERA5 values with NWP forecasts made at multiple lead times, we average the forecast climatologies over lead times of 6 to 120 hours, and normalize by the number of model initializations (i.e., 5). Genesis densities use a contour interval of 2 events per season.

Genesis skill

The case study of the 2023 LPS presented above suggested that NWP models may have the valuable ability to predict the formation of LPS in advance of their actual occurrence. Of the 223 LPS events recorded between 2008 and 2022 in the ERA5 dataset, the GFS-US model successfully predicted roughly 50% of these events about a day prior to the observed genesis (Figure 3a; this fraction is referred to as the Probability of Detection [POD]). As described in the Data and Methods section, model forecasts made at a certain time period prior to observed genesis include forecasts with various lead times. Therefore, POD provides the likelihood that an observed genesis event will be predicted by any forecast, within a given time period before the observed genesis. The GFS-IITM model exhibits similar POD values as the GFS-US model, with the caveat that our assessment of the GFS-IITM model only starts from the year 2016. The ECMWF model has POD values that are higher than those of the GFS-US model by about 0.1 at almost all lead times. Across the three models, the POD decreases rapidly as the forecasts extend further in time from the observed genesis events, with only around 10% of observed genesis events captured 5 days prior to their observed genesis time. Although the ECMWF model had a higher POD over the entire 2008–2022 period, the skill of the GFS-US model seems to be improving over the years, with the POD increasing by about 0.02 per year, which is significant at a 95% confidence level (Figure 3b).

The shorter time period considered for the GFS-IITM model makes it challenging to ascertain changes in its POD values, and the ECMWF model does not exhibit a detectable POD trend.

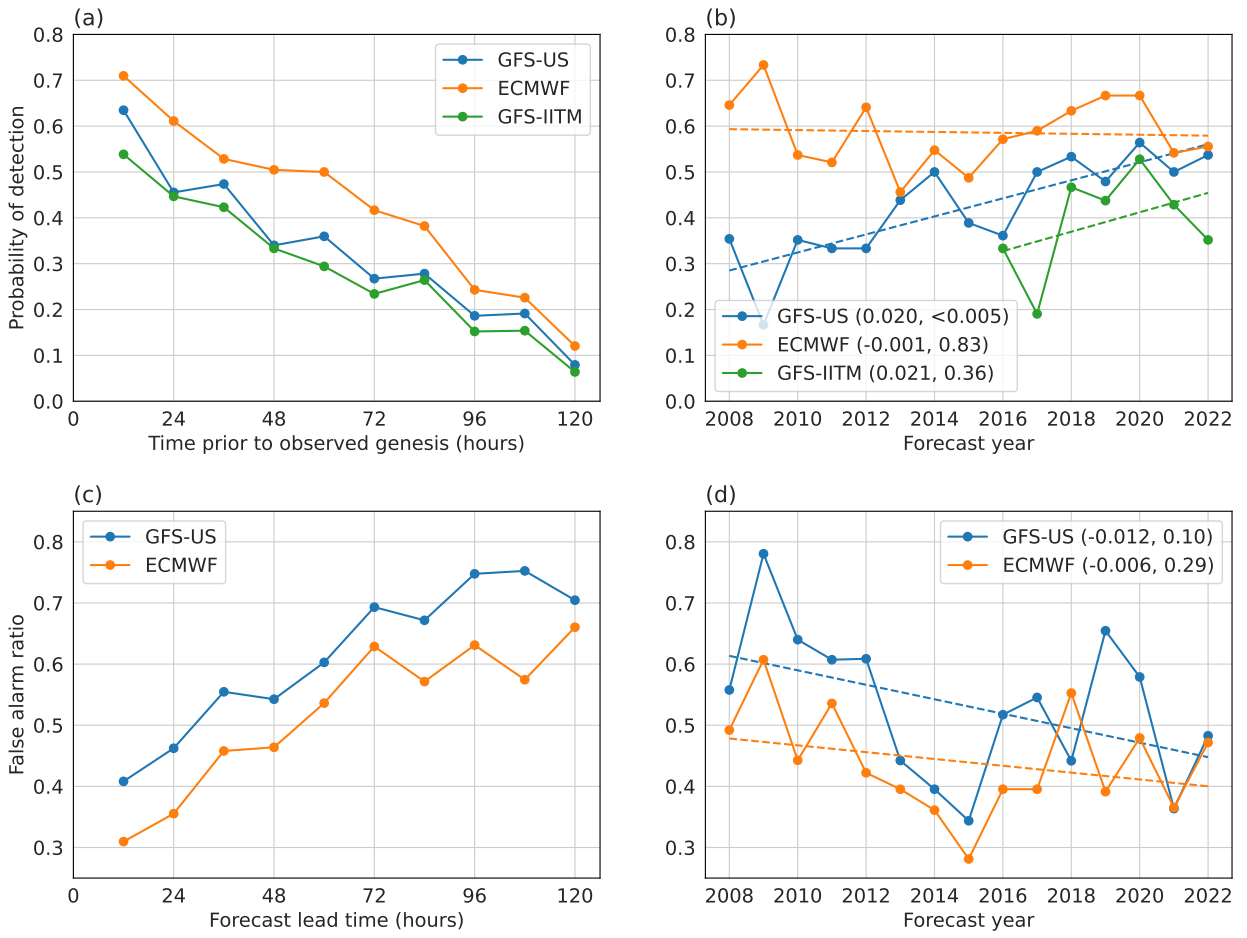

FIG. 3. Top panels show the probability of detection (POD), (a) as a function of time prior to observed genesis, and (b) averaged up to 3 days prior to the observed genesis, as a function of forecast year. Bottom panels show the false alarm ratio (FAR), (c) as a function of model forecast lead time, and (d) averaged over lead times up to 3 days, as a function of forecast year. Dashed lines in the right panels depict linear trends, with slopes (units: year^{-1}) followed by p-values in parentheses in the legends. The p-values are calculated using a two-tailed t-test to evaluate the null hypothesis that the coefficient is equal to zero. For the GFS-US and the ECMWF models, POD and FAR are evaluated over the years 2008–2022. For GFS-IITM, POD is evaluated over 2016–2022, while FAR is not evaluated due to the unavailability of data for all days in the season (see Data and Methods section). As described in the text, POD is estimated as a function of hours prior to observed genesis (as represented in ERA5), while FAR is evaluated as function of model forecast lead time.

Model skill in forecasting genesis depends not only on POD, but also on the number of false alarms, defined as LPS forecast by an NWP model that do not match any observed LPS. The false alarm ratio (FAR), which is the proportion of false alarms to total forecasts made, is about 0.45 for the GFS-US model at a lead time of 1 day (Figure 3c). The ECMWF model exhibits FAR values that are lower than those of the GFS-US model by about 0.1. In both models, the FAR increases with forecast lead time, as expected, with values reaching around 0.7 for a lead time of 5 days. The FAR of the GFS-US model improves over the period of record, although the linear trend has a p-value of 0.10 (Figure 3d); p value of the negative trend in the ECMWF model's FAR is 0.29. As discussed in the Methods section, we did not assess the FAR for the GFS-IITM model due to the lack of availability of data for all summer days. We did, however, repeat our POD and FAR analysis using MERRA-2 instead of ERA5 data, and found obtained similar results (Figure S1 in the online supplementary materials; cf. Figure 3).

Track position and intensity bias

We now assess the skill of model forecasts of LPS track position, which is key to using an NWP forecast to project hazard risk for a region. As expected, position bias increases with forecast lead time (Figure 4a), with this bias defined as the deviation of the forecast LPS track location from the ERA5 track location. For lead times up to around three days, the mean position bias is within 250 km for both models, which is about 10% of the outer diameter of a typical LPS (Hurley and Boos 2015). While the ECMWF model has a slightly smaller mean bias in track position, this distinction remains modest in comparison to the typical storm diameter. The GFS-IITM model shows a bias similar to that of the GFS-US model for lead times up to 3 days; at longer lead times, it exhibits greater biases than the GFS-US model, although the difference is small compared to the standard deviation of these biases (Figure S2 in the online supplementary materials). Over the 2008–2022 period, both the ECMWF and GFS-US models improve in the accuracy of their track forecasts (Figure 4d; linear trend p-values are 0.06 and 0.01, respectively). The improvement in the GFS-US model is largest, with the position bias decreasing by approximately 3 km annually.

Although most previous studies on the hydrological effects of LPS have not distinguished between monsoon lows and monsoon depressions (e.g. Ajayamohan et al. 2010; Goswami et al. 2006; You and Ting 2021), recent work has shown that depressions rain more (Vishnu et al. 2023b) and that

more South Asian disasters are associated with depressions than with lows, even though lows occur more frequently (Suhas et al. 2023). Thus, accurate prediction of LPS intensity is important for disaster prediction. The intensity of an LPS is classified according to the strength of its MSLP anomaly and its peak surface wind speed. Specifically, an LPS is classified as a monsoon depression if the pressure drop (defined above in the case study) exceeds 4 hPa and the surface wind speeds exceed 8.5 m s^{-1} within 3° great circle distance of the storm center(Vishnu et al. 2020; Hurley and Boos 2015; Ajayamohan et al. 2010).

ECMWF forecasts perform better in predicting the pressure drop, with the mean bias of the pressure drop nearing zero across most lead times (Figure 4b). Conversely, the GFS-US model consistently underestimates intensity across all lead times. The roughly 1 hPa average magnitude of this bias results in some of the LPS being classified in the GFS-US forecasts as lows rather than depressions. For instance, the GFS-US model accurately identified 22% of the ERA5 depressions as depressions for times up to 3 days before the observed genesis, while that fraction was 33% for the ECMWF model. Nonetheless, the pressure drop bias in the GFS-US model improved over time and has become similar to the bias in the ECMWF model in recent years (Figure 4e). When evaluated only over the period 2016–2022, the GFS-US model is approximately unbiased in its forecasts of pressure drop for lead times of less than 4 days (Figure S2 in the online supplementary materials). The GFS-IITM model exhibited poorer performance than the GFS-US model at most lead times in this 2016–2022 period, underestimating pressure drops like the GFS-US model did in the earlier 2008–2015 period (Figure S2 in the online supplementary materials).

Forecasts of surface wind speed maxima were approximately unbiased in both the GFS-US and ECMWF models (Figure 4c), as well as the GFS-IITM model (Figure S2 in the online supplementary materials), with mean biases around 0.5 m s^{-1} or less in magnitude. While the GFS-US model slightly underestimated pressure drops, it slightly overestimated the maximum wind speeds. This suggests that the bias in pressure drop was the main factor leading to the GFS-US model categorizing many ERA5 monsoon depressions as lows. It is possible that the wind speed criterion for classification as a depression is often satisfied for LPS because of proximity to the climatological mean low-level monsoon westerlies, which routinely exceed that minimum 8.5 m s^{-1} threshold (see scatterometer-derived surface winds displayed for eight LPS in Cohen and

Boos 2014). Thus, our estimates of intensity bias based on pressure drop may be more meaningful than those based on wind speed.

We repeated this assessment of forecast skill of position, pressure drop, and peak surface wind speed using MERRA-2 data as the reference instead of ERA5. The magnitude of the pressure drop bias increased, with the GFS-US model underestimating the pressure drop by slightly more than 1 hPa instead of slightly less, and the ECMWF model underestimating the pressure drop by about 0.5 hPa (Figure S3 in the online supplementary materials). Also, peak surface wind speeds in MERRA-2 LPS seem to be slightly higher than in ERA5 LPS, which shifts the bias curves in Figure 4c downward by about 0.3 hPa when comparing with MERRA-2. Overall, however, this skill analysis is relatively insensitive to the choice of reference dataset.

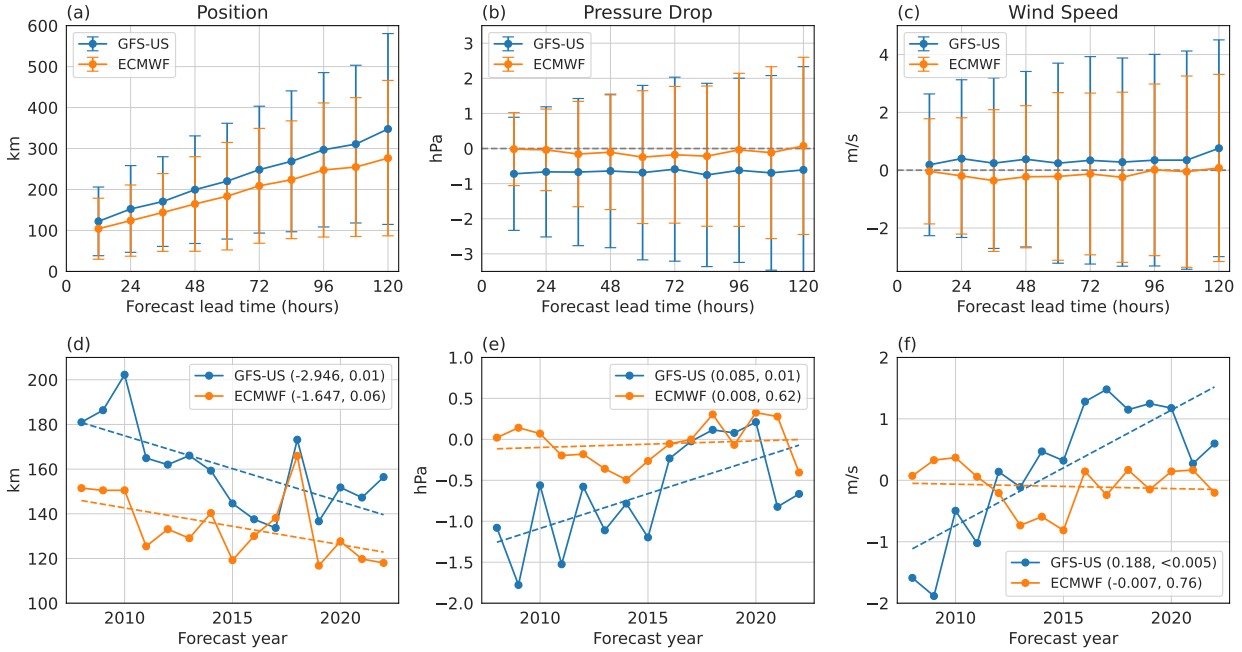

FIG. 4. Top row shows bias as a function of forecast lead time in (a) track position, (b) pressure drop, and (c) maximum surface wind speed for the GFS-US and ECMWF models. These biases are assessed by comparing the forecasts of the NWP models with the ERA5 reanalysis data, and computed over the years 2008–2022. Mean values are represented by solid lines, with standard deviations indicated by error bars. Bottom row, panels (d)-(f), shows biases in the same quantities averaged over lead times of up to 3 days, as function of forecast year. Dashed lines in the bottom panels depict linear trends, with slopes and p-values indicated in the legend.

Precipitation bias

Accurately predicting LPS rainfall is essential for effective disaster preparedness, as more than 50% of hydrological disasters in South Asia during summer are associated with LPS events (Suhas et al. 2023). The NWP models capture the observed peak in rainfall to the southwest of the vortex center, but they underestimate its magnitude by around 20% to 40% and forecast its position further to the east than is observed, when averaging over forecast lead times up to 72 hours and comparing with IMERG precipitation estimates (Figures 5a and b; the asymmetric zonal dipole in the anomaly indicates a weakening and eastward shift relative to observations). Many of the CMIP6 HighResMIP models also simulated LPS peak precipitation that is located closer to the storm center than in observations (Vishnu et al. 2023a).

When precipitation is horizontally averaged over a 5° circle around the storm center, a region that encompasses the typical location of the peak rainfall in the southwest quadrant of LPS (e.g. Sanders 1984; Sikka 2006), both the GFS-US and ECMWF models show only a slight underestimation of precipitation across all lead times (Figure 5c). While the ECMWF model exhibits smaller precipitation biases for lead times beyond 2 days, the spread (here measured by the standard deviation) of bias in this horizontally averaged rainfall is large compared to the mean bias in both models, so these inter-model differences may not be especially meaningful. There are also no statistically significant improvements in precipitation forecasts over the years for both GFS-US and ECMWF models (not shown). Both the GFS-US and ECMWF models also have difficulty forecasting the most intense rain rates. For instance, scatter plots of horizontal mean precipitation averaged over the first three days of lead time reveal that nearly all forecasts underestimate rain rates exceeding 1 mm hr^{-1} in observations (Figure 5d). However, these models more accurately predict moderate rain rates, as evidenced by the peak in the joint histogram of forecast and observed rain rates lying along the 1:1 line (Figure 5d).

Summary and Discussion

Monsoon LPS produce a large fraction of annual rainfall over South Asia (Godbole 1977; Yoon and Chen 2005; Hurley and Boos 2015; Hunt and Fletcher 2019), and leads to extreme precipitation (Ajayamohan et al. 2010) and hydro-metorological disasters (Suhas et al. 2023) in that region. Forecasts of LPS tracks, dynamical intensities, and precipitation made several days

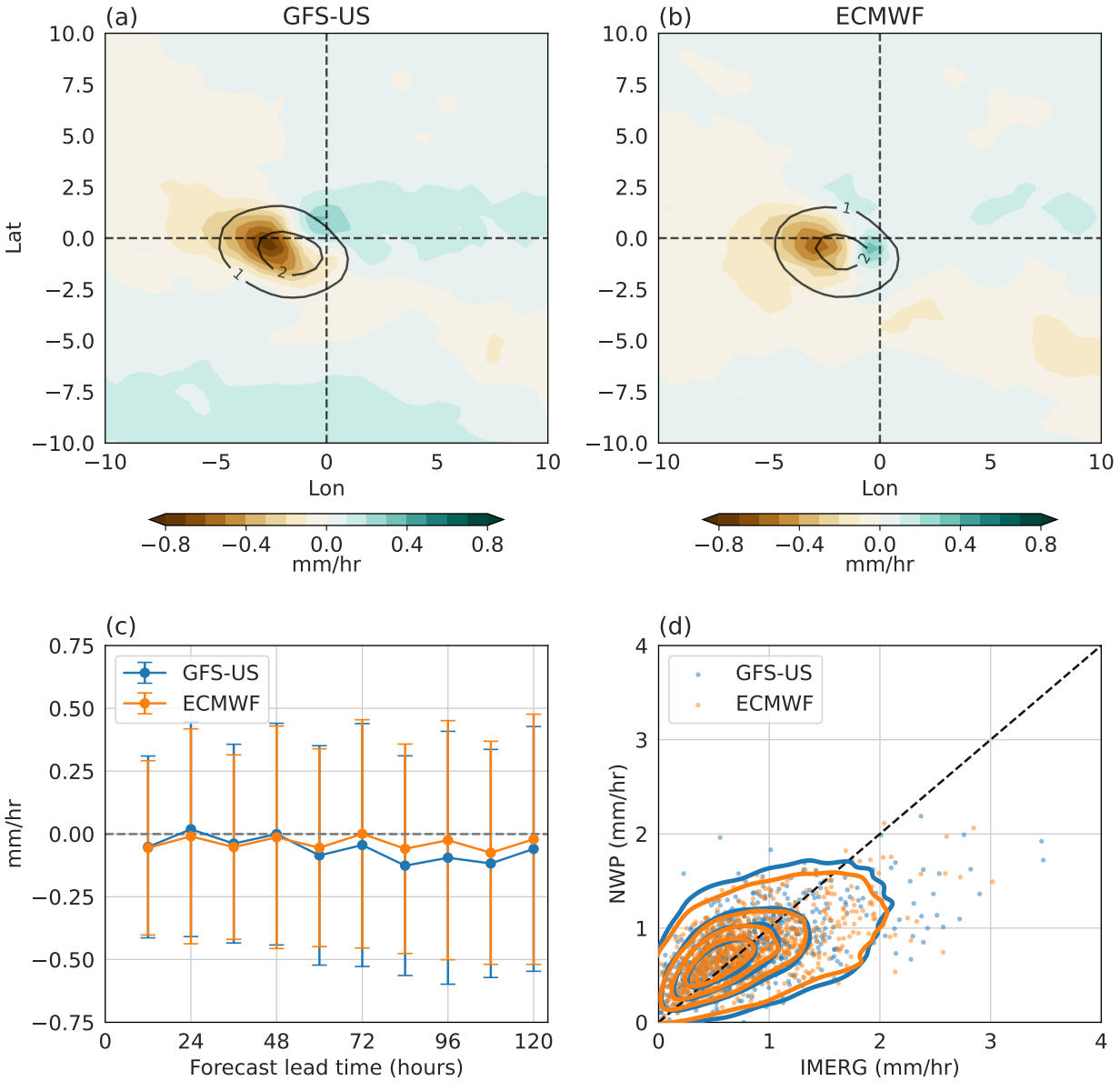

FIG. 5. Storm-centered mean precipitation biases for the (a) GFS-US and (b) ECMWF models, averaged over forecast lead times of up to 72 hours. Observed IMERG precipitation values are shown in black contours, with an interval of 1 mm/hr. Note that IMERG precipitation differs slightly between (a) and (b) because it is averaged over the time period in which the observed and forecast LPS tracks both exist, and this common period differs between forecast models. In panel (c), precipitation biases spatially averaged within 5° of the LPS center are shown as a function of forecast lead time; error bars represent one standard deviation. Panel (d) compares the spatially averaged precipitation from IMERG (horizontal axis) with that forecast by the GFS-US (blue) and ECMWF (orange) models, averaged over forecast lead times up to 72 hours (vertical axis). Contours show kernel density estimates, with individual LPS shown as points; for clarity, only one in 10 data points is shown. Bias is computed using IMERG precipitation at the LPS track locations in ERA5.

before the onset of such disasters may be useful in early warning systems and enhancing disaster preparedness (Suhas et al. 2023). However, to date there has been no operational, automated, real-time tracking of LPS by an objective algorithm that has been well validated for these storms. The new automated forecasting system described here fills this important gap by forecasting LPS tracks using output from NWP models run operationally in the U.S. and India.

In this article, we introduced the features of our automated operational LPS forecast system using a case study of a monsoon LPS that formed over the Bay of Bengal on 24 June 2023 and then produced floods that killed over 200 people. The GFS-US model successfully predicted the genesis of this LPS more than two days in advance, and produced reasonable track and precipitation forecasts. For instance, in a model forecast initialized on 22 June, the automated system projected 150–300 cm of accumulated precipitation over central India over the subsequent 5–7 days, and peak rain rates around 50 mm hr^{-1}, consistent with observations.

We assessed the historical skill of control runs of NWP models in forecasting LPS behavior, using 15 years of forecasts spanning 2008–2022. The genesis and track densities from both the GFS-US and ECMWF models closely resemble the densities in ERA5, which in turn match other reanalyses and a subjectively analyzed track dataset (Vishnu et al. 2020). However, the GFS-US model was only able to successfully predict roughly half of the observed genesis events about a day prior to the actual event, with the ECMWF model successfully predicting an additional 10% of observed genesis events. The ECMWF model also had a lower false alarm ratio of about 0.35 for 1-day lead time, compared to GFS's 0.45. However, the GFS-US model's skill in forecasting genesis improved over time, becoming indistinguishable from the ECMWF model skill in the last 3-5 years. This helps justify the use of GFS-US forecasts in our operational LPS prediction scheme, especially since GFS-US forecasts are publicly available in real time while ECMWF forecasts are not. The LPS genesis skills in these models are in the range of skills found for NWP forecasts of tropical cyclone genesis, although there are substantial variations in tropical cyclone genesis skills across different basins (Halperin et al. 2013, 2016; Zhang et al. 2023).

Both the GFS-US and ECMWF models predict the mean position of LPS within 400 km of the observed (i.e., the reanalyzed) position for lead times of up to five days; this a factor of two or more smaller than the typical storm outer radius of about 1000 km. This position bias is comparable to that of NWP forecasts of stronger tropical cyclones across various operational NWP

models in India (Das et al. 2015; Nadimpalli et al. 2020; Routray et al. 2017). The GFS-US model underestimated the pressure drop (i.e. the dynamical intensity) of LPS by about 1 hPa, resulting in some depressions being wrongly forecast as lows. It is unclear whether this underestimation of intensity is caused by the climatological mean dry bias in that model over India (e.g., perhaps because that dry bias suppresses moist convection which would otherwise lead to intensification), the model's initialization procedure, its subgrid-scale physics, or some other factor. However, this bias is consistent with the finding by Sarkar et al. (2021) that the transition of LPS from lows to depressions occurs too infrequently in the GFS-IITM model. Fortunately, the GFS-US model exhibited improved skill in forecasting track positions and intensities as the years have progressed.

Perhaps the most important quantity examined here is precipitation, which was forecast in a broadly similar fashion by the GFS-US and ECMWF models. While both models capture the peak precipitation to the southwest of the vortex center, they underestimate the peak precipitation by about 40% for the GFS-US model, with somewhat better performance seen in the ECMWF model. Both models also underestimate the most extreme LPS precipitation, i.e., observed horizontal-mean rain rates larger than 1.5 mm hour^{-1} . This behavior at high observed rain rates provides a clear target for bias correction, although the small number of such high-precipitation events may make that task difficult.

These results establish the practical utility of this set of NWP models in forecasting monsoon LPS over South Asia. Given the societal importance of extreme precipitation in LPS (Suhas et al. 2023) and the biases in LPS precipitation forecasts by these models, improvement or statistical bias correction of these models is desirable. Although the task of identifying the cause of these model biases lies outside the scope of this study, future work may assess the possible roles of forecast initialization, model physics, and the climatological dry bias over India in the GFS-US forecasts. Alternatively, LPS properties might be forecast using statistical or machine learning algorithms instead of dynamical NWP models. The results presented here provide a reference level of skill that such algorithms would likely aim for to be of practical use.

Data availability statement. GFS-US data used for real-time operational forecasting is available at `https://www.ncei.noaa.gov/products/weather-climate-models/global-ensemble-forecast`. For the historical skill analysis, GFS-US and the ECMWF forecasts were downloaded from the TIGGE (The International Grand Global Ensemble) archive

(https://apps.ecmwf.int/datasets/data/tigge); TIGGE is an initiative of the World Weather Research Programme (WWRP). GFS-IITM model forecasts were obtained from the Indian Institute of Tropical Meteorology (IITM). ERA5 data was obtained from the Copernicus Climate Change Service (C3S) Climate Data Store (CDS) website (https://cds.climate.copernicus.eu/cdsapp#!/home). The MERRA-2 data set was downloaded from NASA's Goddard Earth Sciences Data and Information Services Center (GES DISC) website (https://gmao.gsfc.nasa.gov/reanalysis/MERRA-2/data_access). IMERG precipitation data is available at https://gpm.nasa.gov/data/directory.

References

Ajayamohan, R., W. J. Merryfield, and V. V. Kharin, 2010: Increasing trend of synoptic activity and its relationship with extreme rain events over central india. *Journal of Climate*, **23 (4)**, 1004–1013.

ANI, 2023: Himachal pradesh: Heavy rainfall disrupts normal life in shimla. *ANI News*, URL https://www.aninews.in/news/national/general-news/himachal-pradesh-heavy-rainfall-disrupts-normal-life-in-shimla20230627215837.

Bechtold, P., J.-P. Chaboureau, A. Beljaars, A. Betts, M. Köhler, M. Miller, and J.-L. Redelsperger, 2004: The simulation of the diurnal cycle of convective precipitation over land in a global model. *Quarterly Journal of the Royal Meteorological Society: A journal of the atmospheric sciences, applied meteorology and physical oceanography*, **130 (604)**, 3119–3137.

Bougeault, P., and Coauthors, 2010: The THORPEX Interactive Grand Global Ensemble. *Bulletin of the American Meteorological Society*, **91 (8)**, 1059–1072, https://doi.org/10.1175/2010BAMS2853.1.

Cangialosi, J. P., 2021: National hurricane center forecast verification report : 2020 hurricane season. *NOAA/National Hurricane Center*.

Chakraborty, A., 2016: A synoptic-scale perspective of heavy rainfall over chennai in november 2015. *Current Science*, 201–207.

Cohen, N. Y., and W. R. Boos, 2014: Has the number of indian summer monsoon depressions decreased over the last 30 years? *Geophysical Research Letters*, **41 (22)**, 7846–7853.

Das, A., Y. Rama Rao, V. Tallapragada, Z. Zhang, S. Roy Bhowmik, and A. Sharma, 2015: Evaluation of the hurricane weather research and forecasting (hwrf) model for tropical cyclone forecasts over the north indian ocean (nio). *Natural Hazards*, **75**, 1205–1221.

Davidson, N., and G. Holland, 1987: A diagnostic analysis of two intense monsoon depressions over australia. *Monthly weather review*, **115 (2)**, 380–392.

Deoras, A., K. M. Hunt, and A. G. Turner, 2021: Comparison of the prediction of indian monsoon low pressure systems by subseasonal-to-seasonal prediction models. *Weather and Forecasting*, **36 (3)**, 859–877.

Dobhal, D., A. K. Gupta, M. Manish, D. Khandelwal, and Coauthors, 2013: Kedarnath disaster: Facts and plausible causes. *Current science*, **105 (2)**, 171–174.

Dubey, C. S., D. P. Shukla, A. Ningreichon, and A. L. Usham, 2013: Orographic control of the kedarnath disaster. *Current Science*, **105 (11)**, 1474–1476.

Froude, L. S., 2010: Tigge: Comparison of the prediction of northern hemisphere extratropical cyclones by different ensemble prediction systems. *Weather and Forecasting*, **25 (3)**, 819–836.

Ganai, M., R. P. M. Krishna, P. Mukhopadhyay, and M. Mahakur, 2016: The impact of revised simplified arakawa-schubert scheme on the simulation of mean and diurnal variability associated with active and break phases of indian summer monsoon using cfsv2. *Journal of Geophysical Research: Atmospheres*, **121 (16)**, 9301–9323.

Godbole, R. V., 1977: The composite structure of the monsoon depression. *Tellus*, **29 (1)**, 25–40.

Goswami, B. N., V. Venugopal, D. Sengupta, M. Madhusoodanan, and P. K. Xavier, 2006: Increasing trend of extreme rain events over india in a warming environment. *Science*, **314 (5804)**, 1442–1445.

Guha-Sapir, D., R. Below, and P. Hoyois, 2015: EM-DAT: International disaster database. *Catholic University of Louvain: Brussels, Belgium*, **27 (2015)**, 57–58.

Halperin, D. J., H. E. Fuelberg, R. E. Hart, and J. H. Cossuth, 2016: Verification of tropical cyclone genesis forecasts from global numerical models: Comparisons between the north atlantic and eastern north pacific basins. *Weather and Forecasting*, **31 (3)**, 947–955.

Halperin, D. J., H. E. Fuelberg, R. E. Hart, J. H. Cossuth, P. Sura, and R. J. Pasch, 2013: An evaluation of tropical cyclone genesis forecasts from global numerical models. *Weather and Forecasting*, **28 (6)**, 1423–1445.

Han, J., and H.-L. Pan, 2011: Revision of convection and vertical diffusion schemes in the ncep global forecast system. *Weather and Forecasting*, **26 (4)**, 520–533.

Hodges, K. I., and R. Emerton, 2015: The prediction of northern hemisphere tropical cyclone extended life cycles by the ecmwf ensemble and deterministic prediction systems. part i: Tropical cyclone stage. *Monthly Weather Review*, **143 (12)**, 5091–5114.

Houze, R., K. Rasmussen, S. Medina, S. Brodzik, and U. Romatschke, 2011: Anomalous atmospheric events leading to the summer 2010 floods in pakistan. *Bulletin of the American Meteorological Society*, **92 (3)**, 291–298.

Houze, R. A., L. McMurdie, K. Rasmussen, A. Kumar, and M. Chaplin, 2017: Multiscale aspects of the storm producing the june 2013 flooding in uttarakhand, india. *Monthly Weather Review*, **145 (11)**, 4447–4466.

Huffman, G. J., D. T. Bolvin, E. J. Nelkin, and J. Tan, 2015: Integrated multi-satellite retrievals for gpm (imerg) technical documentation. *NASA/GSFC Code*, **612 (47)**, 2019.

Hunt, K. M., and J. K. Fletcher, 2019: The relationship between indian monsoon rainfall and low-pressure systems. *Climate Dynamics*, **53 (3)**, 1859–1871.

Hunt, K. M., and A. Menon, 2020: The 2018 kerala floods: a climate change perspective. *Climate Dynamics*, **54 (3)**, 2433–2446.

Hurley, J. V., and W. R. Boos, 2015: A global climatology of monsoon low-pressure systems. *Quarterly Journal of the Royal Meteorological Society*, **141 (689)**, 1049–1064.

IMD, 2023a: Press release : India meteorological department. *India Meteorological Department*, URL https://internal.imd.gov.in/press_release/20230623_pr_2393.pdf.

IMD, 2023b: Press release : India meteorological department. *India Meteorological Department*, URL https://internal.imd.gov.in/press_release/20230624_pr_2394.pdf.

Kumar, A., J. Dudhia, R. Rotunno, D. Niyogi, and U. Mohanty, 2008: Analysis of the 26 july 2005 heavy rain event over mumbai, india using the weather research and forecasting (wrf) model. *Quarterly Journal of the Royal Meteorological Society*, **134 (636)**, 1897–1910.

Mooley, D., and J. Shukla, 1987: *Characteristics of the westward-moving summer monsoon low pressure systems over the Indian region and their relationship with the monsoon rainfall*. Centre for Ocean-Land-Atmosphere Interactions, University of Maryland, College Park, MD, USA.

Mukhopadhyay, P., and Coauthors, 2019: Performance of a very high-resolution global forecast system model (gfs t1534) at 12.5 km over the indian region during the 2016–2017 monsoon seasons. *Journal of Earth System Science*, **128 (6)**, 1–18.

Nadimpalli, R., K. K. Osuri, U. Mohanty, A. K. Das, A. Kumar, S. Sil, and D. Niyogi, 2020: Forecasting tropical cyclones in the bay of bengal using quasi-operational wrf and hwrf modeling systems: an assessment study. *Meteorology and Atmospheric Physics*, **132**, 1–17.

Nikumbh, A. C., A. Chakraborty, G. Bhat, and D. M. Frierson, 2020: Large-scale extreme rainfall-producing synoptic systems of the indian summer monsoon. *Geophysical Research Letters*, **47 (11)**, e2020GL088 403.

Park, Y.-Y., R. Buizza, and M. Leutbecher, 2008: Tigge: Preliminary results on comparing and combining ensembles. *Quarterly Journal of the Royal Meteorological Society: A journal of the atmospheric sciences, applied meteorology and physical oceanography*, **134 (637)**, 2029–2050.

Prasad, V., C. Johny, and J. S. Sodhi, 2016: Impact of 3d var gsi-enkf hybrid data assimilation system. *Journal of Earth System Science*, **125 (8)**, 1509–1521.

Rao, K., and S. Rajamani, 1970: Diagnostic study of a monsoon depression by geostrophic baroclinic model.

Routray, A., V. Singh, J. P. George, S. Mohandas, and E. Rajagopal, 2017: Simulation of tropical cyclones over bay of bengal with ncmrwf regional unified model. *Pure and Applied Geophysics*, **174**, 1101–1119.

Sampson, C. R., and A. J. Schrader, 2000: The automated tropical cyclone forecasting system (version 3.2). *Bulletin of the American Meteorological Society*, **81 (6)**, 1231–1240.

Sanders, F., 1984: Quasi-geostrophic diagnosis of the monsoon depression of 5–8 july 1979. *Journal of Atmospheric Sciences*, **41 (4)**, 538–552.

Sarkar, S., P. Mukhopadhyay, S. Dutta, R. Phani Murali Krishna, R. D. Kanase, V. Prasad, and M. S. Deshpande, 2021: Gfs model fidelity in capturing the transition of low-pressure area to monsoon depression. *Quarterly Journal of the Royal Meteorological Society*.

Sati, S., and V. Gahalaut, 2013: The fury of the floods in the north-west himalayan region: the kedarnath tragedy. *Geomatics, Natural Hazards and Risk*, **4 (3)**, 193–201.

Sikka, D., 1978: Some aspects of the life history, structure and movement of monsoon depressions. *Monsoon dynamics*, Springer, 1501–1529.

Sikka, D., 2006: *A study on the monsoon low pressure systems over the Indian region and their relationship with drought and excess monsoon seasonal rainfall*. Center for Ocean-Land-Atmosphere Studies.

Suhas, D., and W. Boos, 2024: Evaluation of the genesis skill of south asian monsoon low pressure systems in two global ensemble models. *NA*, **NA (NA)**.

Suhas, D. L., N. Ramesh, R. M. Kripa, and W. R. Boos, 2023: Influence of monsoon low pressure systems on south asian disasters and implications for disaster prediction. *npj Climate and Atmospheric Science*, **6 (1)**, 48.

Swinbank, R., and Coauthors, 2016: The tigge project and its achievements. *Bulletin of the American Meteorological Society*, **97 (1)**, 49–67.

The Weather Channel, 2023: Weather today (june 27): Heavy to very heavy rains to lash himachal, gujarat, madhya maharashtra, goa, kerala. *The Weather Channel*, URL https://weather.com/en-IN/india/news/news/2023-06-27-weather-today-june-27-very-heavy-rain-in-himachal-maharashtra.

Thomas, T. M., G. Bala, and V. V. Srinivas, 2021: Characteristics of the monsoon low pressure systems in the indian subcontinent and the associated extreme precipitation events. *Climate Dynamics*, **56 (5)**, 1859–1878.

Tiedtke, M., 1989: A comprehensive mass flux scheme for cumulus parameterization in large-scale models. *Monthly weather review*, **117 (8)**, 1779–1800.

Times, L. A., 2023: Record monsoon rains kill more than 100 people in northern india. *Los Angeles Times*, URL https://www.latimes.com/world-nation/story/2023-07-13/record-monsoon-rains-kill-100-people-northern-india.

Ullrich, P. A., C. M. Zarzycki, E. E. McClenny, M. C. Pinheiro, A. M. Stansfield, and K. A. Reed, 2021: Tempestextremes v2. 1: a community framework for feature detection, tracking, and analysis in large datasets. *Geoscientific Model Development*, **14 (8)**, 5023–5048.

Vishnu, S., W. Boos, and W. Collins, 2023a: Historical and future trends in south asian monsoon low pressure systems in a high-resolution model ensemble. *npj Clim Atmos Sci*, **182 (6)**.

Vishnu, S., W. Boos, P. Ullrich, and T. O'Brien, 2020: Assessing historical variability of south asian monsoon lows and depressions with an optimized tracking algorithm. *Journal of Geophysical Research: Atmospheres*.

Vishnu, S., M. D. Risser, T. A. O'Brien, P. A. Ullrich, and W. R. Boos, 2023b: Observed increase in the peak rain rates of monsoon depressions. *npj Climate and Atmospheric Science*, **6 (1)**, 111.

Yoon, J.-H., and T.-C. Chen, 2005: Water vapor budget of the indian monsoon depression. *Tellus A: Dynamic Meteorology and Oceanography*, **57 (5)**, 770–782.

You, Y., and M. Ting, 2021: Observed trends in the south asian monsoon low-pressure systems and rainfall extremes since the late 1970s. *Geophysical Research Letters*, **48 (9)**, e2021GL092 378.

Yu, H., P. Chen, Q. Li, and B. Tang, 2013: Current capability of operational numerical models in predicting tropical cyclone intensity in the western north pacific. *Weather and forecasting*, **28 (2)**, 353–367.

Zhang, X., J. Fang, and Z. Yu, 2023: The forecast skill of tropical cyclone genesis in two global ensembles. *Weather and Forecasting*, **38 (1)**, 83–97.

Zhou, X., and Coauthors, 2022: The development of the ncep global ensemble forecast system version 12. *Weather and Forecasting*, **37 (6)**, 1069–1084.